A Reference-Feed-Forward-Based Damping Method for Virtual Synchronous Generator Control

Yu, Yun; Chaudhary, Sanjay K.; Agundis-Tinajero, Gibran D.; Xu, Luona; Abu Bakar, Nur Najihah Binti; Vasquez, Juan; Guerrero, Josep M.

Published in:
IEEE Transactions on Power Electronics

DOI (link to publication from Publisher):
10.1109/TPEL.2022.3152358

Publication date:
2022

Document Version
Accepted author manuscript, peer reviewed version

A Reference-Feed-Forward-Based Damping Method for Virtual Synchronous Generator Control

Yun Yu *Student Member, IEEE*, Sanjay K Chaudhary *Senior Member, IEEE*, Gibran David Agundis Tinajero *Member, IEEE*, Luona Xu *Student Member, IEEE*, Nur Najihah Binti Abu Bakar *Member, IEEE*, Juan C. Vasquez *Senior Member, IEEE*, and Josep M. Guerrero *Fellow, IEEE*

***Abstract*—The virtual synchronous generator (VSG) control has been extensively applied for realizing grid-friendly interconnections of power converters. Nevertheless, due to the direct shaft dynamics emulation, low-frequency power oscillations may be introduced in the case of limited damping effects. To solve this issue, power control law modifications have been proposed based on the feedback control theory. Although power oscillations can be suppressed to an acceptable level, the original inertial response of VSG will be significantly degraded. This paper proposes a new damping method based on the reference feed forward (RFF) control. The proposed method is able to effectively attenuate poorly-damped power oscillations in VSG-controlled converters without affecting the original inertial response. Theoretical analysis and effectiveness of the proposed damping method have been validated by both EMT simulations and experiments.**

***Index Terms*—Virtual synchronous generator (VSG), power oscillation, oscillation damping, reference feed forward control**

I. Introduction

VSG has been applied in various applications to enable islanded operation, inertial response and frequency support [1]–[3]. However, the virtual inertia embedded in VSGs may introduce low-frequency active power oscillations, which subsequently affects the system stability and increase the risk of damaging power electronic converters [4], [5].

In order to suppress the low-frequency active power oscillations, various damping algorithms have been developed [6]–[10]. In [6], additional damping effects have been realized by using the frequency slip estimated from a phase-locked loop (PLL). One problem of using this PLL-based method is the PLL-related stability issue, especially when grids are weak [11]. Additionally, without the help of PLLs, a damping correction control approach was proposed in [7], where the algorithm was developed based on modifying the active power feedback. Although acceptable attenuation of power oscillations can be attained by adjusting the filter passband, the degrees of freedom are limited to achieve fully adjustable power dynamics. Benefiting from the flexibility of state-feedback control, the method proposed in [8] enables fully controllable power dynamics. Moreover, the damping approach derived from the relationship between power dynamics and angular accelerations was proposed in [9]. It is able to provide fully controllable power dynamics for individual VSG as well as parallel connected VSGs. In [10], another approach was proposed by adding a virtual damping element.

One common disadvantage of aforementioned methods is that the damping term based on the feedback control inevitably affects the original inertial response of VSG [12]. Specifically, when loads change rapidly, the rate of change of frequency (RoCoF) can not be limited by inertia as desired [12]. To solve this issue, this paper proposes a new damping method using the feed forward control, and its technical contributions can be summarized as: i) No degradation of the inertial response; ii) Fully controllable damping effects and power dynamics; iii) Enable automatic tuning and real-time adaptation, in the case that system parameters are measured or estimated.

The rest of the paper is organized as follows. In Section II, the small-signal model is presented. In Section III, power oscillations and existing damping algorithms are analyzed. Section IV introduces the proposed RFF-based damping method. In Section V, simulation and experimental results are given, which leads to the final conclusion in Section VI.

II. Modeling of the VSG-Controlled System

Fig. 1 indicates the general scheme of a VSG, where R_f and L_f are converter-side resistor and inductor, and C_f denotes the filter capacitor. The impedance of the interconnection transformer is denoted by Z_t, the grid impedance is represented by Z_g, and $Z_L = Z_t + Z_g$ is the total grid-side impedance.

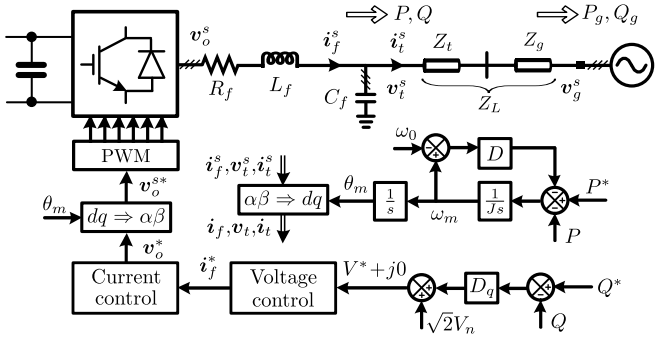

Fig. 1. Simplified diagram of a VSG-controlled converter.

Manuscript received September 19, 2021; revised November 8, 2021, December 28, 2021 and February 1, 2022; accepted February 12, 2022. This work was supported by VILLUM FONDEN under the VILLUM Investigator Grant (No. 25920), Ministry of Foreign Affairs of Denmark, Danida Fellowship Centre (No. 19-M03-AAU) and China Scholarship Council. *(Corresponding author: Yun Yu)*

The authors are with the Center of Research on Microgrids, AAU Energy, Aalborg University, 9220 Aalborg, Denmark (e-mail: yyu@energy.aau.dk; skc@energy.aau.dk; gdat@energy.aau.dk; lxu@energy.aau.dk; nurnbab@energy.aau.dk; juq@energy.aau.dk; joz@energy.aau.dk).

As depicted in Fig. 1, the active power transferred by the VSG is regulated by the swing equation as follows:

$$P^* - P = J\frac{d\omega_m}{dt} + D\left(\omega_m - \omega_0\right) \tag{1}$$

where J and D denote inertia and droop coefficients for active power regulation, respectively. ω_m is the angular frequency of the VSG, and ω_0 represents the normal grid frequency.

From Fig. 1, VSG's instantaneous active and reactive power can be formulated as [13]

$$\begin{aligned} P &= 3/2\left(v_{td}i_{td} + v_{tq}i_{tq}\right), \\ Q &= 3/2\left(v_{tq}i_{td} - v_{td}i_{tq}\right) \end{aligned} \tag{2}$$

where v_{td}, v_{tq}, i_{td} and i_{tq} are capacitor voltage and grid-side current on the synchronous dq coordinates.

However, for modeling a VSG, (2) normally leads to a high-order model which includes all the dynamics of current and voltage loops [14], and this inevitably makes analysis and controller design complex. Without loss of generality, impacts of inner control loops can be neglected for simplicity, assuming that the bandwidth of these loops is much higher than that of power control loops [4], [8], [9], [15]. The VSG-controlled system is assumed to be balanced in most cases as well. Subsequently, the analysis can be conducted by using the phasor representation, where capacitor and grid voltage phasors are denoted by $\dot{V}_t = V_t\angle\delta$ and $\dot{V}_g = V_g\angle 0$, respectively, and δ is the power angle which can be expressed as

$$\delta = \int \left(\omega_m - \omega_g\right) dt \tag{3}$$

where ω_g is the angular frequency of the grid voltage.

Assuming that the grid-side impedance is mainly inductive, Z_L can be then replaced by the reactance X_L. Note that, if the grid-side network is not mainly inductive, a virtual impedance loop can be used for adjusting the equivalent output impedance to be mainly inductive [16]. Active and reactive power of the VSG-controlled converter can be subsequently obtained from the phasor representation as [17]

$$\begin{aligned} P &= 3V_tV_g\sin(\delta)/X_L, \\ Q &= 3\left[V_t^2 - V_tV_g\cos(\delta)\right]/X_L. \end{aligned} \tag{4}$$

Since δ is normally small enough, approximation $\sin\delta \approx \delta$ and $\cos\delta \approx 1$ can be applied. In addition, $V_t \approx V_g \approx V_n$, where V_n denotes the rated phase voltage. It should be mentioned that, in the case of unbalanced conditions, (4) cannot be used to replace (2), a different modeling method should be applied.

With respect to the low-frequency power oscillation issue in the VSG-controlled converter, analyses are generally applied without considering the reactive power control since the oscillation is mainly introduced by the active power control [4], [8], [9], [18], i.e., using a large virtual inertia. In this manner, power loops are taken as fully decoupled, and only active power dynamics are included the analysis. By linearizing (1), (3), and (4), the small-signal model of the active power change ΔP over the set point variation ΔP^* is derived as [9], [15]

$$\Delta P = \frac{3V_n^2}{JX_Ls^2 + DX_Ls + 3V_n^2}\Delta P^*. \tag{5}$$

TABLE I
VARIANTS OF THE SWING EQUATION

Ref.	Active power control law	ADOF	$\frac{\Delta P}{\Delta P^*}$
[6]	$P^*-P=J\frac{d\omega_m}{dt}+D(\omega_m-\omega_0)+D_{pll}\left(\omega_m-\hat{\omega}_g\right)$	1	2^{nd}
[7]	$P^*-\frac{1+D_fs}{1+T_fs}P=J\frac{d\omega_m}{dt}+D(\omega_m-\omega_0)$	2	3^{th}
[8]	$P^*-\frac{1}{1+T_fs}P=J\frac{d\omega_m}{dt}+D(\omega_m-\omega_0)-P_d$ $P_d=k_{x\omega}(\omega_m-\omega_0)+\frac{k_{xp}}{1+T_fs}P+\frac{k_{xi}}{s}P_d$	4	4^{th}
[9]	$P^*-\left(\frac{k_{p1}s}{s+k_{p2}}+1\right)P=\left(J+\frac{k_{\omega 1}}{s+k_{\omega 2}}\right)\frac{d\omega_m}{dt}+D(\omega_m-\omega_0)$	4	4^{th}
[10]	$P^*-P=J\frac{d\omega_m}{dt}+D(\omega_m-\omega_0)+D_v\left(\frac{T_\omega s}{s+T_\omega}\right)\omega_m$	2	3^{th}

III. Low-Frequency Power Oscillations Damping

From (5), it can be seen that power dynamics are determined once coefficient J is chosen for a desired inertia response and coefficient D is fixed according to the P–f droop curve. Since there are no more degrees of freedom (DOF) for tuning the overall damping level, low-frequency power oscillations may appear in the VSG-controlled converter. For extra damping effects to attenuate oscillations, variants of the swing equation have been extensively proposed, as summarized in Table I.

It worth noting that only when the additional DOF (ADOF) introduced by extra damping terms is greater than or equal to the order of $\Delta P/\Delta P^*$, closed-loop poles can be freely adjusted as desired without changing coefficients J and D. Thus, only the variants developed in [8], [9] provide enough ADOF. Nevertheless, all the algorithms in Table I will introduce degradation of the inertial response [12]. For a better damping method, the requirements are twofold:

1) No degradation of the inertial response.
2) Provide enough ADOF for any desired damping level and power dynamic.

IV. RFF-Based Damping Methods

To introduce enough damping effects on active power oscillations without affecting the inertial response, RFF control is utilized. As shown in Fig. 2, VSG's active power is regulated by both RFF terms and the classical swing equation.

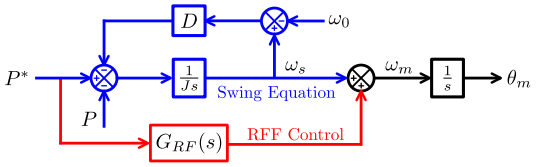

Fig. 2. Active power control with proposed RFF-based damping method.

From Fig. 2, VSG's new active power control law can be expressed as follows:

$$\begin{aligned} P^* - P &= J\frac{d\omega_s}{dt} + D\left(\omega_s - \omega_0\right), \\ \omega_m &= \omega_s + P^*G_{RF}\left(s\right). \end{aligned} \tag{6}$$

where ω_s is the swing-equation-regulated angular frequency .

In the steady state, for no impact on the static droop characteristic determined by the coefficient D, the RFF controller

$G_{RF}(s)$ should filter out most low frequency contents in the power reference, and one possible solution is as follows:

$$G_{RF1}(s) = k_{hp1}\frac{s}{s+k_{hp2}} \tag{7}$$

where k_{hp1} and k_{hp2} are two coefficients for adjusting the pass band of the RFF control loop. Combine (3), (4), (6) and (7), the following small-signal model can be derived:

$$\Delta P = \frac{3V_n^2\left[Jk_{hp1}s^2 + (Dk_{hp1}+1)s + k_{hp2}\right]}{(JX_Ls^2 + DX_Ls + 3V_n^2)(s+k_{hp2})}\Delta P^* \tag{8}$$

Here an additional real pole is introduced at $-k_{hp2}$. There are two extra zeros can be adjusted by both k_{hp1} and k_{hp2}. For adequate damping effects, two zeros need to be moved towards the poorly-damped poles. It is better to place the zeros along the natural frequency curve of those poles. In this way, the effect of zeros can mitigate the oscillations generated by the poorly-damped poles to the most extent. As shown in Fig. 3, a sweep of k_{hp1} is conducted for the best pole-zero placement.

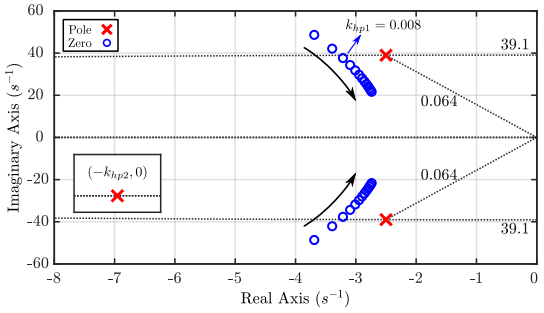

Fig. 3. Pole-zero map of $\Delta P/\Delta P^*$, where k_{hp1} varies from 0.006 to 0.03, $k_{hp2}=1000$, $J=70$, $D=350$, $V_n=380/\sqrt{3}$ V, and $X_L = 1.35\ \Omega$.

Although poorly-damped oscillations can be eased by placing additional zeros, the ADOF is still limited for tuning the damping effect. Therefore, for adjusting power dynamics to any desired level, controller $G_{RF}(s)$ can be directly derived by assuming $\Delta P/\Delta P^*$ is a second order plant as

$$\Delta P = \frac{\omega_n^2}{s^2 + 2\zeta\omega_n s + \omega_n^2}\Delta P^* \tag{9}$$

where ζ is the desired damping factor, and ω_n is the desired natural frequency. From (3), (4), (6) and (9), the RFF controller $G_{RF}(s)$ can be directly derived as follows:

$$G_{RF2}(s) = \frac{m_2 s^2 + m_1 s}{3V_n^2\left(Js^3 + n_2 s^2 + n_1 s + D\omega_n^2\right)} \tag{10}$$

where the coefficients in (10) are

$$\begin{aligned} m_2 &= J\omega_n^2 X_L - 3V_n^2, \quad m_1 = D\omega_n^2 X_L - 6V_n^2\zeta\omega_n, \\ n_2 &= D + 2J\zeta\omega_n, \quad n_1 = J\omega_n^2 + 2D\zeta\omega_n. \end{aligned} \tag{11}$$

From (11), it can be seen that all the controller coefficients are calculated directly according to parameters of the VSG-controlled system, damping factor ζ and natural frequency ω_n, which significantly benefits the controller automatic tuning and real-time adaptation. With respect to the selection of ζ and ω_n, the classical criteria which is normally used for tuning second-order plants can be adopted. For well-damped active power responses, the damping factor ζ can be set to a value greater than 0.7. Afterwards, the natural frequency ω_n can be selected according to the settling time requirement, i.e., $\omega_n = T_{set}\zeta/4$, where T_{set} is the settling time [19].

It should be mentioned that the aforementioned theoretical analysis is conducted under the assumption that active and reactive power loops of a VSG are fully decoupled; however, it cannot be ensured in some cases [15]. Therefore, it is necessary to assess the coupling effect of VSG's reactive power loop on the proposed scheme. Taking the coupling effect into account, the small-signal model of the active power loop can be written as

$$\Delta P = \frac{3V_n^2\left[1 + (Js+D)G_{RF}(s)\right]T_c}{JX_Ls^2 + DX_Ls + 3V_n^2T_c}\Delta P^* \tag{12}$$

where T_c represents the coupling effect which is introduced by the reactive power loop. The derivation of (12) and T_c are given in the Appendix.

Using (7), (10) and (12), the impact of the power-loop coupling can be assessed by the pole-zero map of $\Delta P/\Delta P^*$. To have a convincing evaluation of the coupling effect, the static power angle δ_n in (A.3) is firstly set to a large value, for instance, 1 rad. The droop gain D_q in (A.2) varies from 0 pu to 10 pu. As shown in Fig. 4, either RFF controller $G_{RF1}(s)$ or $G_{RF2}(s)$ is applied, the coupling effect on the effectiveness of improving the overall damping level can be neglected since the desired pole-zero placement is barely changed by D_q.

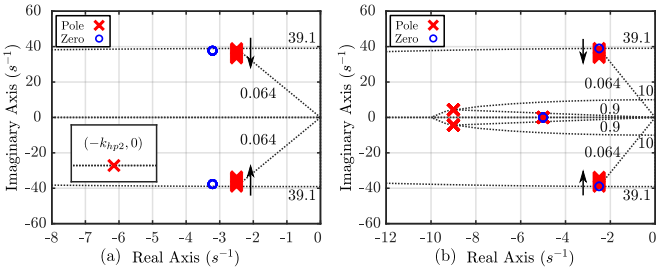

Fig. 4. Pole-zero map of $\Delta P/\Delta P^*$ when $\delta_n=1$ rad, and D_q changes from 0 pu to 10 pu. $J=70$, $D=350$, $V_n=380/\sqrt{3}$ V, and $X_L = 1.35\ \Omega$. (a) Controller $G_{RF1}(s)$ is applied with k_{hp1}=0.008 and k_{hp2}=1000; (b) Controller $G_{RF2}(s)$ is applied with $\zeta=0.9$ and $\omega_n=10$ rad/s.

V. Simulation and Experimental Validations

To validate the effectiveness of proposed RFF-based damping method, EMT simulations based on the averaged value of converters have been conducted in Digsilent/PowerFactory, and a laboratory implementation as Fig. 5 is performed as well. In the studies, two cases shown in Fig. 6 have been included, and the active power is obtained via the instantaneous calculation as (2). All the parameters used in the studies are listed in Table II.

A. Damping of low-frequency oscillations - Simulation

In the simulation studies, the grid-tied mode is tested firstly. A step change from 0 to 0.6 pu is applied in the active power set point. As shown in Fig. 7(a), without any additional damping terms, output oscillates at a low frequency (around

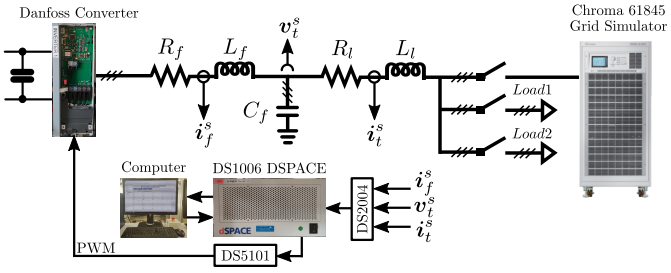

Fig. 5. Experiment setup.

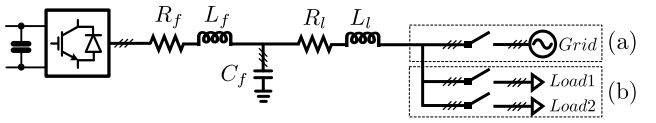

Fig. 6. Circuit diagrams of two cases. (a) Damping of low-frequency power oscillations in grid-tied mode; (b) Inertial response in islanded mode.

6 Hz). However, when $G_{RF1}(s)$ is applied with k_{hp1}=0.008 and k_{hp2}=1000, damping effects are significantly improved. Especially, with $G_{RF2}(s)$ applied with $\zeta = 0.9$ and $\omega_n = 10$ rad/s, poorly-damped oscillations are attenuated to zero.

B. The inertial response - Simulation

To check the inertial response, the approach used in [4] and the RoCoF calculation method specified in [20] are adopted. The VSG initially supplies 0.6 kW local load, and a step change of 0.6 kW is suddenly applied in the local load to simulate the load variation. The resulting angular frequencies are shown in Fig. 7(b). It can be seen that angular frequencies change in the same way, with or without the proposed RFF-based damping method, and the values of RoCoF are approximately the same. The results indicate that the inertial response of VSG is well preserved.

C. Damping of low-frequency oscillations - Experiment

A step change of 0.6 kW is applied in the active power set point of grid-tied VSG to demonstrate power oscillations. As

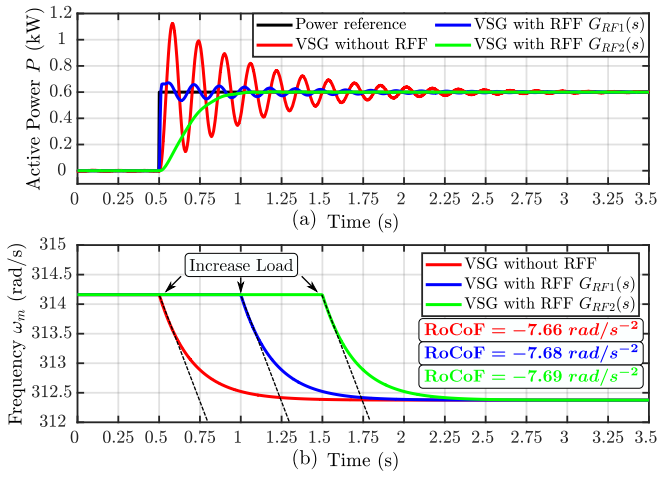

Fig. 7. Simulation results (a) VSG output active power in grid-tied mode; (b) VSG angular frequency in islanded mode.

TABLE II
PARAMETERS OF THE VSG-CONTROLLED CONVERTER

Symbol	Values simulation	Values experiment	Symbol	Values simulation	Values experiment
S_{base}	2.2 kVA	2.2 kVA	V_n	$380/\sqrt{3}$ V	$380/\sqrt{3}$ V
ω_0	314 rad/s	314 rad/s	V_{dc}	650 V	650 V
R_f	0 Ω	0.1 Ω	L_f	3.6 mH	3.6 mH
C_f	9 μF	9 μF	R_l	0 Ω	0.5 Ω
L_l	4.3 mH	4.3 mH	f_{sw}	N/A	10 kHz
J	70 (10 pu)	70 (10 pu)	D	350 (50 pu)	350 (50 pu)
D_q	0.014 (0.1 pu)	0.014 (0.1 pu)			
k_{hp1}	0.008	0.03	k_{hp2}	1000	1000
ζ	0.9	0.9	ω_n	10 rad/s	10 rad/s

shown in Fig 8(a), after the set point change, oscillations at approximately 4 Hz appear in the output power. Because of inevitable mismatches in the setup, for example, impedance variations, sampling errors and nonlinear properties of the power converter, the oscillation frequency is not exactly the same as that in the simulation. The difference is around 2 Hz. However, it does not affect the experimental assessment.

As shown in Fig. 8(b), when the $G_{RF1}(s)$ is applied with k_{hp1}=0.03 and k_{hp2}=1000, low-frequency power oscillations can be significantly attenuated as the simulation result shown in Fig. 7. The difference between simulation ($k_{hp1} = 0.008$) and experimental (k_{hp1}=0.03) settings reveals that controller $G_{RF1}(s)$ is sensitive to the parameter variations. Thus, for appropriate damping effects, an accurate placement of zeros introduced by $G_{RF1}(s)$ is essential. In this manner, an optimization method may be required in real applications when $G_{RF1}(s)$ is applied to VSGs. On the other hand, experimental results presented in Fig. 8(c) show that controller $G_{RF2}(s)$ is still effective under the same condition. The coefficients ζ and ω_n are set to 0.9 and 10 rad/s in both simulation and experiment. As depicted in Fig. 8(c), smooth power dynamics without any overshoot and oscillation can be attained, which is the same as the result obtained in the simulation studies.

D. The inertial response - Experiment

The VSG operates in islanded mode, and one resistor bank of 230 Ω is used as the local load. Another 230 Ω resistor bank is switched on to emulate a sudden load variation, just as the scenario applied in [4]. As shown in Fig. 9, with or without using the proposed RFF-based damping method, angular frequencies of VSG change in the same profile. Especially, the values of RoCoF are almost the same, which shows that the inertial response of VSG is not changed.

E. Response to the grid frequency variation - Experiment

For a further assessment of the proposed control scheme under grid frequency variations, a step frequency change of 0.2 Hz is applied in the experiment. VSGs are connected to the grid, and the grid frequency drops suddenly from the nominal value 50 Hz to 49.8 Hz. As shown in Fig. 10, responses of grid-tied VSGs with or without feedforward controllers are approximately the same. Specifically, at the moment of frequency step change, power angle δ in (4) starts to increase,

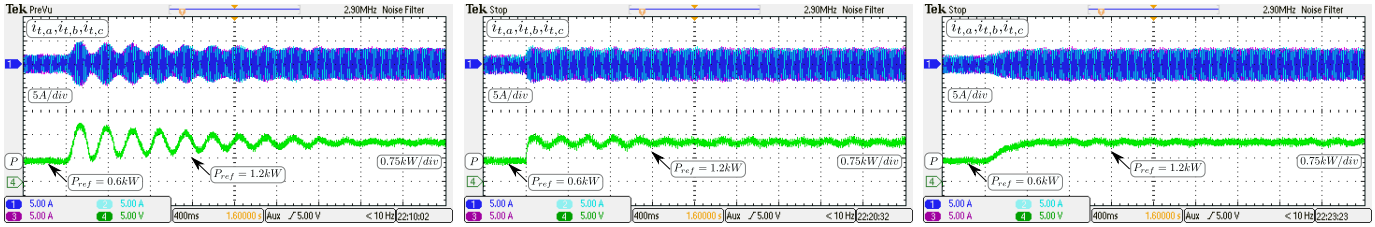

(a) (b) (c)

Fig. 8. Waveforms of the grid-tied VSG. (a) Without proposed damping methods; (b) Controller $G_{RF1}(s)$ is applied; (c) Controller $G_{RF2}(s)$ is applied.

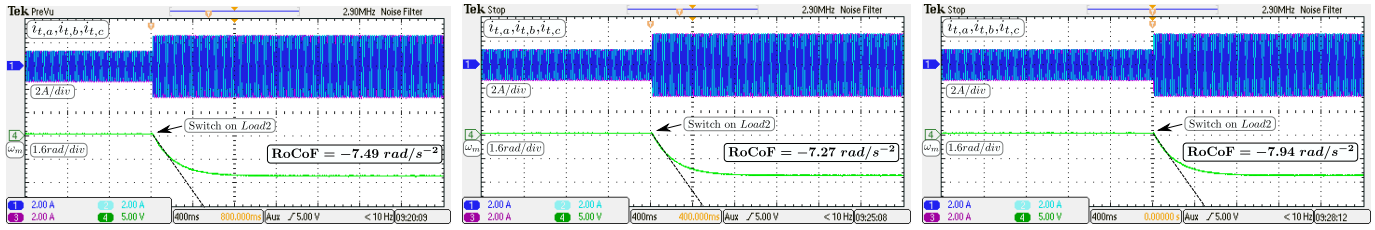

(a) (b) (c)

Fig. 9. Waveforms of the islanded VSG. (a) Without proposed damping methods; (b) Controller $G_{RF1}(s)$ is applied; (c) Controller $G_{RF2}(s)$ is applied.

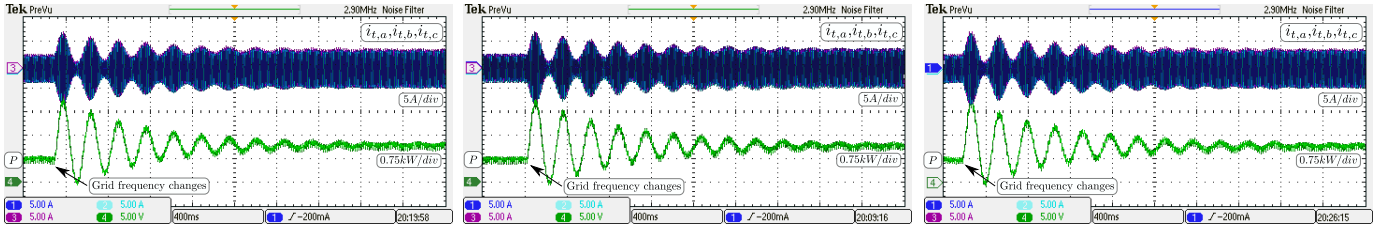

(a) (b) (c)

Fig. 10. Waveforms of the grid-tied VSG under grid frequency variations. (a) Without proposed damping methods; (b) Controller $G_{RF1}(s)$ is applied; (c) Controller $G_{RF2}(s)$ is applied.

and the output power rise rapidly to inject inertial power for supporting the grid frequency. Afterwards, because original inertial responses of tested VSGs are preserved without any degradation, the output power swings until a new operation point is reached.

VI. Conclusion

This paper proposes a simple but effective method to actively attenuate the poorly-damped power oscillations in VSG-controlled converters. Different from the existing algorithms using the feedback control, the proposed method introduces a feed-forward path to improve the damping level. By applying the proposed method, threefold benefits have been attained: i) Power oscillations can be effectively attenuated without affecting the original inertial response; ii) The damping effect and power dynamics can be flexibly adjusted to any specific level; iii) Controller automatic tuning and real-time adaptation are enabled, provided that system parameters are available.

It is worthy to note that, under sudden gird frequency variations, the rapid active power change which comes from the original inertial response is favorable for maintaining the grid frequency stability; nevertheless, the resulting power swings are not necessary. To handle this issue in grid-tied VSGs, additional control strategies could be developed and implemented with the proposed control scheme.

Appendix

From (4), active and reactive power variations, which include the coupling items, can be derived as [15]

$$\begin{aligned}\Delta P &= 3V_n^2\Delta\delta/X_L + 3V_n\left(\Delta V_t + \Delta V_g\right)\delta_n/X_L,\\ \Delta Q &= 3V_n\left(\Delta V_t - \Delta V_g\right)/X_L + 3V_n^2\delta_n\Delta\delta/X_L\end{aligned} \tag{A.1}$$

where δ_n denotes the static power angle.

In (A.1), $\Delta V_g \approx 0$, and ΔV_t can be formulated as

$$\Delta V_t = D_q\left(\Delta Q^* - \Delta Q\right) \tag{A.2}$$

where D_q denotes the droop gain.

Taking both (A.2) and (A.1) into account, the active power variation, which contains the reactive power loop gain, can be rewritten as

$$\Delta P = \frac{3V_n^2}{X_L}\underbrace{\left(1 - \frac{T_q}{1+T_q}\delta_n^2\right)}_{T_c}\Delta\delta \tag{A.3}$$

where T_q is the reactive power loop gain which is equal to $3V_nD_q/X_L$. From (3), (6) and (A.3), the active power change ΔP over the set point variation ΔP^* can be derived as (12).

REFERENCES

[1] J. Liu, Y. Miura, and T. Ise, "Comparison of dynamic characteristics between virtual synchronous generator and droop control in inverter-based distributed generators," *IEEE Trans. Power Electron.*, vol. 31, no. 5, pp. 3600–3611, 2016.

[2] J. Fang, Y. Tang, H. Li, and X. Li, "A battery/ultracapacitor hybrid energy storage system for implementing the power management of virtual synchronous generators," *IEEE Trans. Power Electron.*, vol. 38, no. 4, pp. 2820–2824, 2018.

[3] M. Chen, D. Zhou, and F. Blaabjerg, "Modelling, implementation, and assessment of virtual synchronous generator in power systems," *J. Mod. Power Syst. Clean Energy*, vol. 8, no. 3, pp. 399–411, 2020.

[4] X. Meng, J. Liu, and Z. Liu, "A generalized droop control for grid-supporting inverter based on comparison between traditional droop control and virtual synchronous generator control," *IEEE Trans. Power Electron.*, vol. 34, no. 6, pp. 5416–5438, 2019.

[5] W. Du, Q. Fu, and H. F. Wang, "Power system small-signal angular stability affected by virtual synchronous generators," *IEEE Trans. Power Syst.*, vol. 34, no. 4, p. 3209–3219, 2019.

[6] T. Shintai, Y. Miura, and T. Ise, "Oscillation damping of a distributed generator using a virtual synchronous generator," *IEEE Trans. Power Del.*, vol. 29, no. 2, pp. 668–676, Apr. 2014.

[7] S. Dong and Y. C. Chen, "Adjusting synchronverter dynamic response speed via damping correction loop," *IEEE Trans. Power Electron.*, vol. 32, no. 2, pp. 608–619, Jun. 2017.

[8] J. Liu, Y. Miura, and T. Ise, "Fixed-parameter damping methods of virtual synchronous generator control using state feedback," *IEEE Access*, vol. 7, pp. 99 177–99 190, Jul. 2019.

[9] M. Chen, D. Zhou, and F. Blaabjerg, "Active power oscillation damping based on acceleration control in paralleled virtual synchronous generators system," *IEEE Trans. Power Electron.*, vol. 36, no. 8, pp. 9501–9510, Aug. 2021.

[10] Z. Shuai, W. Huang, Z. J. Shen, A. Luo, and Z. Tian, "Active power oscillation and suppression techniques between two parallel synchronverters during load fluctuations," *IEEE Trans. Power Electron.*, vol. 35, no. 4, pp. 4127–4142, Apr. 2020.

[11] S. Golestan, J. M. Guerrero, and J. C. Vasquez, "Three-phase PLLs: A review of recent advances," *IEEE Trans. Power Electron.*, vol. 32, no. 3, pp. 1894–1907, 2017.

[12] Y. Yu *et al.*, "A comparison of fixed-parameter active-power-oscillation damping solutions for virtual synchronous generators," in *Proc. 47th Annu. Conf. IEEE Ind. Electron. Soc.*, 2021, pp. 1–6.

[13] A. Hirofumi, E. H. Watanabe, and M. Aredes, *Instantaneous power theory and applications to power conditioning*. John Wiley & Sons, 2017.

[14] S. D'Arco, J. A. Suul, and O. B. Fosso, "Automatic tuning of cascaded controllers for power converters using eigenvalue parametric sensitivities," *IEEE Trans. Ind. Appl.*, vol. 51, no. 2, pp. 1743–1753, 2015.

[15] H. Wu *et al.*, "Small-signal modeling and parameters design for virtual synchronous generators," *IEEE Trans. Ind. Electron.*, vol. 63, no. 7, pp. 4292–4303, 2016.

[16] J. He and Y. W. Li, "Analysis, design, and implementation of virtual impedance for power electronics interfaced distributed generation," *IEEE Trans. Ind. Appl.*, vol. 47, no. 6, pp. 2525–2538, 2011.

[17] R. W. Erickson and D. Maksimovic, *Fundamentals of Power Electronics*, 2nd ed. Norwell, MA, USA: Kluwer, 2001.

[18] J. Liu, Y. Miura, and T. Ise, "A comparative study on damping methods of virtual synchronous generator control," in *Proc. Eur. Conf. Power Electron. Appl.*, 2019, pp. 1–10.

[19] R. C. Dorf and R. H. Bishop, *Modern Control Systems*, 12th ed. Englewood Cliffs, NJ, USA:Pearson, 2011.

[20] R. Bugdal, A. Dysko, G. M. Burt, and J. R. McDonald, "Performance analysis of the ROCOF and vector shift methods using a dynamic protection modelling approach," *Proc. Effect Distrib. Gener. Power Syst. Protection*, p. 139–144, 2006.